

20 **Abstract**

21 Enhancements of stationary planetary waves (SPWs) and traveling planetary
22 waves (TPWs) are commonly observed in the middle atmosphere during sudden
23 stratospheric warming (SSW) events. Based on the least-square fitting method (Wu et
24 al., 1995), numerous studies have used satellite measurements to investigate the
25 characteristics of TPWs during SSWs but ignored the effect of the SPWs. However, a
26 rapid and large change in the SPWs during SSWs may lead to significant disturbances
27 in the amplitude of derived TPWs. In this study, we present a new methodology for
28 obtaining the amplitudes and wavenumbers of traveling quasi-5-day oscillations
29 (Q5DOs) in the middle atmosphere during major SSWs. Our new fitting method is
30 developed by inhibiting the effect of a rapid and large change in SPWs during SSWs.
31 We demonstrate the effectiveness of the new method using both synthetic data and
32 satellite observations. The results of the simulations indicate that the new method can
33 suppress the aliasing from SPWs and capture the real variations of TPWs during SSWs.
34 Based on the geopotential height data measured by the Aura satellite from 2004 to 2021,
35 the variations of traveling Q5DOs during eight mid-winter major SSWs are reevaluated
36 using the new method. The differences in the fitted amplitudes between the least-square
37 fitting method and the new method are usually over 100 m during the SSW onsets. Our
38 analysis indicates that previously-reported Q5DOs during SSWs might be
39 contaminated by SPWs, which leads to both overestimation and underestimation in the
40 amplitudes of the traveling Q5DOs.

41

42 **1. Introduction**

43 Sudden stratospheric warming (SSW) is one of the most representative phenomena
44 in the atmospheric dynamics in the polar region, which is excited by the interaction
45 between stationary planetary waves (SPWs) and background mean flow (Matsuno,
46 1971; Baldwin et al., 2021). The onset of SSW is characterized by a positive gradient
47 of zonal mean temperature between 90°N and 60°N at 10 hPa (Andrews et al., 1987).
48 Generally, a major SSW event is additionally associated with the phenomenon of wind
49 reversals in the zonal mean eastward winds at 60°N and 10 hPa; otherwise, SSWs are
50 regarded as minor events (Charlton and Polvani, 2007; Butler et al., 2017; Choi et al.,
51 2019). During the occurrence of SSWs, the enhancements of SPWs largely affect the
52 energy transportation in the stratosphere and the occurrence of extreme weather in the
53 troposphere at middle latitudes (e.g., Manney et al., 2009; Kozubek et al., 2015; King
54 et al., 2019; Domeisen et al., 2020). The zonal wavenumber of the enhanced SPWs
55 usually corresponds to the geometry of the polar vortex during SSWs (e.g., Harada and
56 Hirooka, 2017; Liu et al., 2019; White et al., 2021). A displacement vortex is mainly
57 due to a strong SPW with a zonal wavenumber of 1 (SPW1) and split vortices are
58 always associated with large SPWs with a zonal wavenumber of 2 (SPW2) (e.g.,
59 Seviour et al., 2013; Lawrence and Manney, 2018; Choi et al., 2019).

60 Traveling planetary waves (TPWs), widely observed with strong amplitudes
61 during SSWs in recent decades, also play a significant role in controlling the global
62 atmospheric and ionospheric couplings during SSWs (e.g., Gong et al., 2019; Koushik
63 et al., 2020; Lin et al., 2020; Ma et al., 2022). One of the prominent TPWs, the westward

64 propagating quasi-5-day oscillation (Q5DO) with periods of 4-7 days, is usually
65 observed from the mesosphere to the ionosphere at mid-latitudes during SSWs with the
66 zonal wavenumbers both 1 and 2 (W1 and W2) (Gong et al., 2018; Pancheva et al.,
67 2018; Yamazaki et al., 2020, 2021). These Q5DOs are believed to be generated by
68 atmospheric barotropic/baroclinic instability due to large changes in zonal winds and
69 temperatures during SSWs (e.g., Liu et al., 2004; Ma et al., 2020; Yamazaki et al., 2021).
70 Based on the least-square fitting method introduced by Wu et al. (1995), the amplitude,
71 phase, and zonal wavenumber of the Q5DOs can be obtained from satellite observations
72 and reanalysis data sets (e.g., Huang et al., 2017; Qin et al., 2021). However, based on
73 the least-square fitting method, a rapid and large change in the amplitudes of SPWs
74 would lead to an apparent fluctuation in the amplitude of TPWs over a broad range of
75 frequencies, including those corresponding to Q5DOs. Yamazaki and Matthias (2019)
76 proposed that based on the least-square fitting method, the effect of an SPW on a quasi-
77 10-day wave (Q10DW) is equivalent to two oppositely propagating waves with equal
78 amplitudes, periods, and wavenumbers. They suggested that the effect of SPWs can be
79 ignored when the activities of Q10DWs in the oppositely propagating direction were
80 not simultaneously enhanced.

81 However, the rapid change in the amplitudes of SPWs is a typical characteristic
82 during the occurrence of SSWs. Previous studies usually ignored the effect of SPWs
83 when obtaining the amplitudes of Q5DOs from satellite observations (e.g., Gong et al.,
84 2018; Qin et al., 2021). Nevertheless, both westward and eastward Q5DOs have been
85 frequently reported during SSWs in recent years (e.g., Pancheva et al., 2018; Rhodes et

86 al., 2021; Wang et al., 2021; Yu et al., 2022). Thus, it is necessary to understand the real
87 physics of the enhanced Q5DOs during SSWs and their relationships with SPWs. It is
88 also necessary to inhibit the effect of SPWs when studying the variations of Q5DOs
89 during SSWs. In the present study, we develop a new method for measuring the
90 variation of westward and eastward propagating Q5DOs by inhibiting the effect of a
91 rapid and large change in SPWs. The effectiveness of the new method is demonstrated
92 by using both simulations and satellite observations. The paper is organized as follows.
93 In Section 2, the synthetic data and the satellite data used in this study are introduced.
94 Section 3 presents the new methodology for measuring the amplitudes of Q5DOs.
95 Discussions are given in Section 4, mainly focusing on the comparisons of traveling
96 Q5DOs during SSWs between the least-square fitting method and the new fitting
97 method. Conclusions are summarized in section 5.

98 **2. Data**

99 In the present study, a simulation is performed based on synthetic data to further
100 understand the issue of SPWs and Q5DOs during SSWs. The synthetic data $Y(x, t)$
101 are built based on equation (1), including three components: an SPW, a westward
102 propagating Q5DO, and an eastward propagating Q5DO, respectively, which is
103 expressed as:

$$104 Y(x, t) = A_k(t) \cos(kx - \varphi_k) + B_w \cos(\omega t + kx - \varphi_w) + B_e \cos(\omega t - kx - \varphi_e) \quad (1)$$

105 where x is the longitudes, t is the time, k is the wavenumber, ω is the frequency of
106 Q5DOs, A_k and φ_k are the amplitude and phase of SPWs, B_w and B_e denote the

107 amplitudes of westward and eastward Q5DOs with the phase of φ_w and φ_e ,
108 respectively. Based on the least-square fitting method introduced by Wu et al. (1995),
109 TPWs with the same zonal wavenumber but in other periods only cause periodic
110 modulation in the fitted amplitudes of Q5DOs. The aliasing caused by TPWs with
111 different wavenumbers is mainly captured in the studies of quasi-2-day waves based on
112 satellite measurements (Tunbridge et al., 2011). For the analysis of Q5DOs, the aliasing
113 caused by TPWs with different wavenumbers is usually ignored, because Q5DOs with
114 wavenumbers of 3 or 4 are rarely reported. Nevertheless, the most important issue of
115 the least-square fitting method may be the aliasing due to the rapid and large changes
116 in the SPWs. Therefore, to better understand the issue, the synthetic data for the
117 simulations in the present study only includes three components of waves with the same
118 zonal wavenumbers.

119 To verify the effectiveness of different fitting methods, the geopotential height data
120 measured by the Aura/Microwave Limb Sounder (MLS) from 2005 to 2021 are used to
121 derive the Q5DOs in the present study. The available Aura/MLS geopotential height
122 data in the version 4.2x Level 2 product is from 261 hPa to 0.001 hPa (Livesey et al.,
123 2017), with the measurement errors of ± 25 m, ± 45 m, ± 110 m, and ± 160 m at 1 hPa,
124 0.1 hPa, 0.01 hPa, and 0.001 hPa. A comprehensive study of the measurement errors
125 and fitting errors has been reported by Yamazaki and Matthias (2019) when using the
126 Aura/MLS geopotential height data to obtain the amplitudes of Q5DOs. They have
127 suggested that the mean values of the estimated $1-\sigma$ uncertainties in TPWs are about 50
128 m at high latitudes in the Northern Hemisphere. Following their technique, mean values

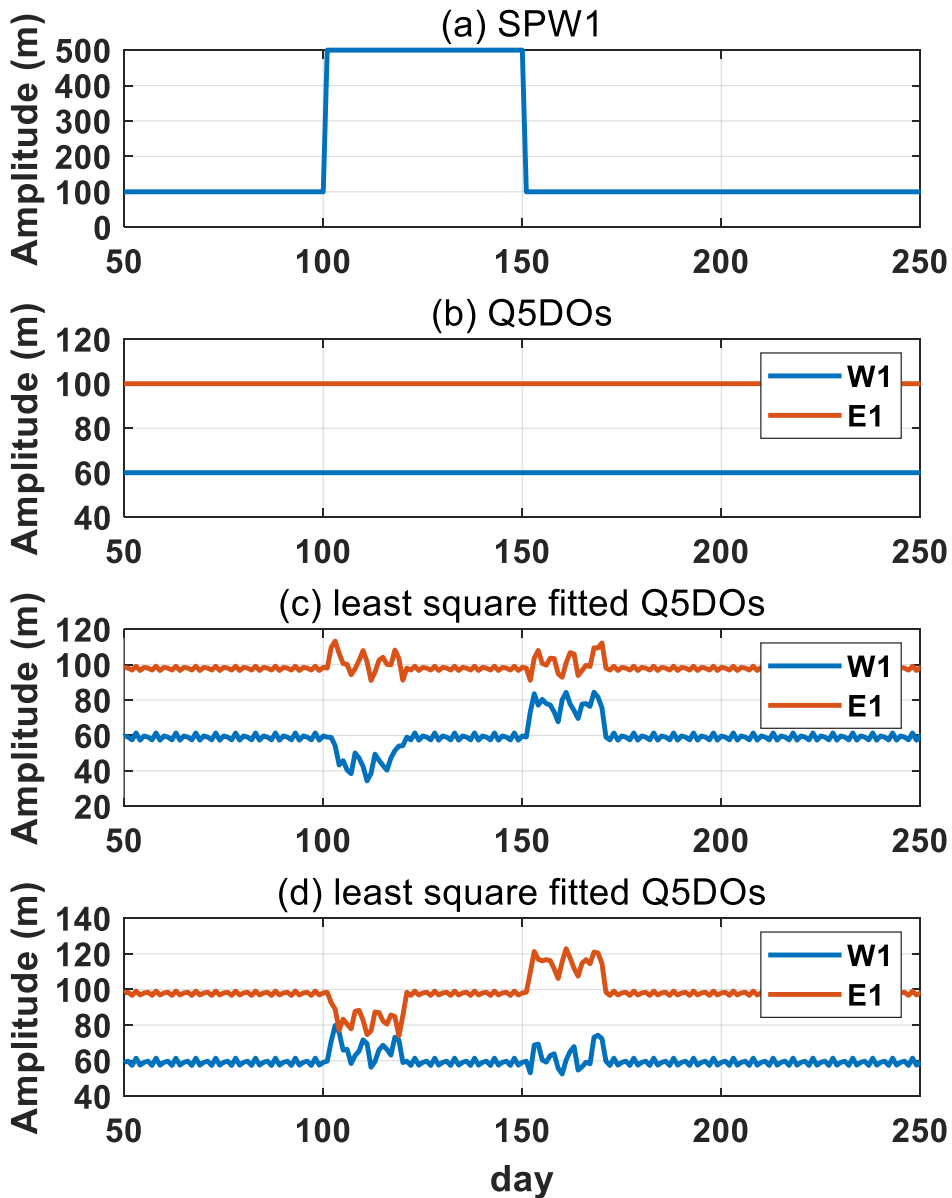
129 of the estimated $1-\sigma$ uncertainties in the fitted amplitudes obtained by the new method
130 are also about 50 m. The vertical structure of the estimated $1-\sigma$ uncertainty of the new
131 method is the same as the distributions shown in Yamazaki and Matthias (Figure 1,
132 2019). In the present study, we focus on the difference between the original and new
133 fitting methods. The fitted amplitudes are presented in the following analyses without
134 dropping the values that are lower than the uncertainties. The analysis of this study
135 focuses on the traveling Q5DOs with zonal wavenumbers of 1 and 2 based on the data
136 at 60°N (averaged from $55\text{-}65^\circ\text{N}$).

137 **3. Methodology**

138 **3.1 Simulations of the least-square fitting method**

139 The least-square fitting method used in previous studies to derive the amplitude
140 and phase of Q5DOs from satellite observations is based on equation (1) but without
141 fitting the first term on the right-hand side (e.g., Huang et al., 2017; Qin et al., 2021).
142 Generally, a 20-day sliding window with a step of one day is used to simultaneously
143 extract the amplitudes of TPWs with zonal wavenumbers from 3 to -3 (westward to
144 eastward). The daily amplitudes of the Q5DOs are obtained with the largest value in
145 the wave periods between 4 and 7 days. The fitting result is marked at the end day of
146 each 20-day window. To better understand the original least-square fitting method, the
147 synthetic data are used to first simulate the effect of a rapid and large change in SPWs
148 when calculating the amplitudes of Q5DOs. As shown in Figures 1a and 1b, three
149 components of waves with the zonal wavenumber of 1 are given in the synthetic data,

150 which are an SPW with the amplitude of 100 m, eastward and westward propagating
 151 Q5DOs with amplitudes of 100 m and 60 m, respectively. The phases are respectively
 152 set as 0 , $-\pi/4$, and $\pi/5$ for the SPW and the westward and eastward propagating Q5DOs.
 153 To simulate the effect of SPWs on TPWs, rapid large changes are given in the
 154 amplitudes of SPW on day 100 with magnitudes from 100 m to 500 m and on day 150
 155 with magnitudes from 500 m to 100 m (see Figure 1a).



156

157 Figure 1. Simulations of the least-square fitting method based on synthetic data, which
158 includes an SPW and westward and eastward Q5DOs with zonal wavenumber of 1. (a)
159 Daily variations of the SPW amplitudes. The phase of the SPW is 0. (b) The real
160 amplitudes of Q5DOs. Amplitudes are separately set as 100 m and 60 m for the
161 eastward and westward Q5DOs. (c) Q5DOs obtained from the least-square fitting
162 method. The phases are $-\pi/4$ and $\pi/5$ for the westward and eastward Q5DOs,
163 respectively. (d) Same as (c) but with phases of $\pi/4$ and $-\pi/5$ for the westward and
164 eastward Q5DOs.

165 Figure 1c presents the amplitudes of the westward and eastward propagating
166 Q5DOs fitted by the least-square fitting method. As shown in Figure 1c, abnormal
167 fluctuations after day 100 and day 150 are captured, which correspond to the occurrence
168 of rapid large changes in the amplitudes of SPW. However, Figure 1c suggests that the
169 fitted Q5DOs are not largely influenced by the SPWs when rapid large changes are not
170 given in the amplitudes of SPWs (before day 100 or from day 120 to 150). Additionally,
171 Figure 1c indicates that abnormal fluctuations in Q5DOs induced by SPWs are not
172 equivalent to two oppositely propagating directions. An enhancement and a decrease in
173 the amplitudes of westward and eastward propagating Q5DOs can be simultaneously
174 observed. Results shown in Figure 1d are the same as that in Figure 1c but are derived
175 based on different phases of the westward and eastward Q5DOs in the synthetic data,
176 where $\pi/4$, and $-\pi/5$ are given in the westward and eastward Q5DOs. Comparing the
177 results between Figures 1c and 1d, it is interesting to note that the effect of a rapid large
178 change in SPWs on the derived Q5DOs also depends on the phase relationships.

179 Yamazaki and Matthias (2019) suggested that the effect of SPWs could be ignored when
 180 the activities of Q10DWs in the oppositely propagating direction were not
 181 simultaneously enhanced. However, according to our simulations, this criterion is not
 182 suitable for the analysis of Q5DOs with different phases. Our simulation indicates that
 183 the influence of a quick and large change of SPW should not be ignored when extracting
 184 Q5DOs during SSWs from satellite observations based on the least-square fitting
 185 method. Thus, in this study, we develop a new fitting method to derive the Q5DOs by
 186 suppressing the effect of a rapid and large change in SPWs.

187 **3.2 New fitting method**

188 Since the daily amplitude of SPW ($A_k(t)$) cannot be directly derived when
 189 Q5DOs exist, the primary goal of the new method is to eliminate the rapid and large
 190 changes in $A_k(t)$. The following steps are performed, where SPWs and Q5DOs are
 191 considered within the same wavenumbers.

192 **Step 1. Estimate the daily variations of SPWs.**

193 Based on the definition of SPW, the phase φ_k should be a fixed value in each
 194 window. Therefore, φ_k is first fitted based on $y(x) = a_k \cos(kx - \varphi_k)$, where $y(x)$
 195 is the time-averaged geopotential height in each 20-day window. Using the fitted phase
 196 φ_k , the daily amplitudes of SPW can be roughly estimated by the least-square fitting
 197 based on equation (2), which equals equation (1).

$$\begin{aligned}
 198 \quad Y(x, t) = & [A_k(t) + B_w \cos(\omega t - \varphi_w + \varphi_k) + B_e \cos(\omega t - \varphi_e - \varphi_k)] \cos(kx - \varphi_k) \\
 199 \quad & + [B_e \sin(\omega t - \varphi_e - \varphi_k) - B_w \sin(\omega t - \varphi_w + \varphi_k)] \sin(kx - \varphi_k) \quad (2)
 \end{aligned}$$

200 If we let $a_k(t) = A_k(t) + B_w \cos(\omega t - \varphi_w + \varphi_k) + B_e \cos(\omega t - \varphi_e - \varphi_k)$, and

201 $b_k(t) = B_e \sin(\omega t - \varphi_e - \varphi_k) - B_w \sin(\omega t - \varphi_w + \varphi_k)$, equation (2) can be simply
 202 expressed as equation (3):

$$203 \quad Y(x, t) = a_k(t) \cos(kx - \varphi_k) + b_k(t) \sin(kx - \varphi_k) \quad (3)$$

204 However, the fitted amplitudes of SPWs, $a_k(t)$, are not the true amplitudes of SPWs
 205 ($A_k(t)$), which includes the aliasing from Q5DOs. According to the above two
 206 equations, rapid and large changes in SPW amplitudes can only have impacts on the
 207 values of $a_k(t)$. Because the true values of $A_k(t)$ cannot be directly fitted due to the
 208 aliasing of Q5DOs, our goal in Step 2 is to eliminate the rapid large changes in $a_k(t)$.

209 **Step 2. Eliminate the large rapid changes in SPWs.**

210 If we let $P_k(t) = B_w \cos(\omega t - \varphi_w + \varphi_k) + B_e \cos(\omega t - \varphi_e - \varphi_k) =$
 211 $P \cos(\omega t - \varphi)$, $a_k(t)$ in Equation (3) can be also expressed as,

$$212 \quad a_k(t) = A_k(t) + P_k(t) = A_k(t) + P \cos(\omega t - \varphi) \quad (4)$$

213 The amplitude P and phase φ can be estimated by the least-square fitting via
 214 equation (4). Taking the partial derivatives in time on both sides of equation (4), we
 215 obtain equation (5):

$$216 \quad \frac{\partial}{\partial t} a_k(t) = \frac{\partial}{\partial t} A_k(t) + \frac{\partial}{\partial t} P_k(t) \quad (5)$$

217 where $\frac{\partial}{\partial t} A_k(t)$ are the daily variations in the amplitudes of SPW. The primary goal of
 218 Step 2 is to subtract large values of $\frac{\partial}{\partial t} A_k(t)$ from $a_k(t)$ to eliminate the large
 219 variations in $a_k(t)$. However, $\frac{\partial}{\partial t} A_k(t)$ cannot be obtained simply by $\frac{\partial}{\partial t} A_k(t) =$
 220 $\frac{\partial}{\partial t} a_k(t) - \frac{\partial}{\partial t} P_k(t)$, because $\frac{\partial}{\partial t} P_k(t)$ cannot be derived accurately when $\left| \frac{\partial}{\partial t} A_k(t) \right|$
 221 are large (“ $| \quad |$ ” represents the absolute values). Nevertheless, the lower boundary of
 222 the values in $\left| \frac{\partial}{\partial t} a_k(t) \right|$ can be estimated when rapid large changes exist in SPWs

223 $\left|\frac{\partial}{\partial t} A_k(t)\right|$ are large). The maximum value in $\left|\frac{\partial}{\partial t} a_k(t)\right|$ will be at least larger than the
 224 maximum value in $\frac{\partial}{\partial t} P_k(t) = -\omega P \sin(\omega t - \varphi)$, which is ωP . Thus, the value of ωP
 225 can be used as a threshold to determine rapid large changes in SPWs.

226 Therefore, when $\left|\frac{\partial}{\partial t} a_k(t)\right|$ are larger than the threshold of ωP , we subtract the
 227 value of the corresponding $\frac{\partial}{\partial t} A_k(t)$ from all the following members of $a_k(t)$ to
 228 obtain a new series of $a_k^{new}(t)$. The $\frac{\partial}{\partial t} A_k(t)$ are estimated by $\frac{\partial}{\partial t} A_k^{estimated}(t) =$
 229 $\frac{\partial}{\partial t} a_k(t) - \frac{\partial}{\partial t} P_k^{estimated}(t)$, where $P_k^{estimated}(t) = P_{pre} \cos(\omega(t + 1) - \varphi_{pre})$.
 230 Instead of the P and φ fitted in the present window, the P_{pre} and φ_{pre} fitted from
 231 the previous one are used because the fitted P_{pre} and φ_{pre} are not influenced by the
 232 effect of rapid large changes in SPWs in the present window. Here, we have a new
 233 series of $a_k^{new}(t)$ without rapid large changes in SPWs, as well as new fitted P and
 234 φ for the next window.

235 **Step 3. Fit the real amplitudes of Q5DOs.**

236 After obtained the $a_k^{new}(t)$ and $b_k(t)$ from Step 2, the reconstruction of the
 237 original data $Y'(x, t)$, which inhibits the rapid and large changes in SPWs, can be
 238 reconstructed based on equation (6):

$$239 \quad Y'(x, t) = a_k^{new}(t) \cos(kx - \varphi_k) + b_k(t) \sin(kx - \varphi_k) \quad (6)$$

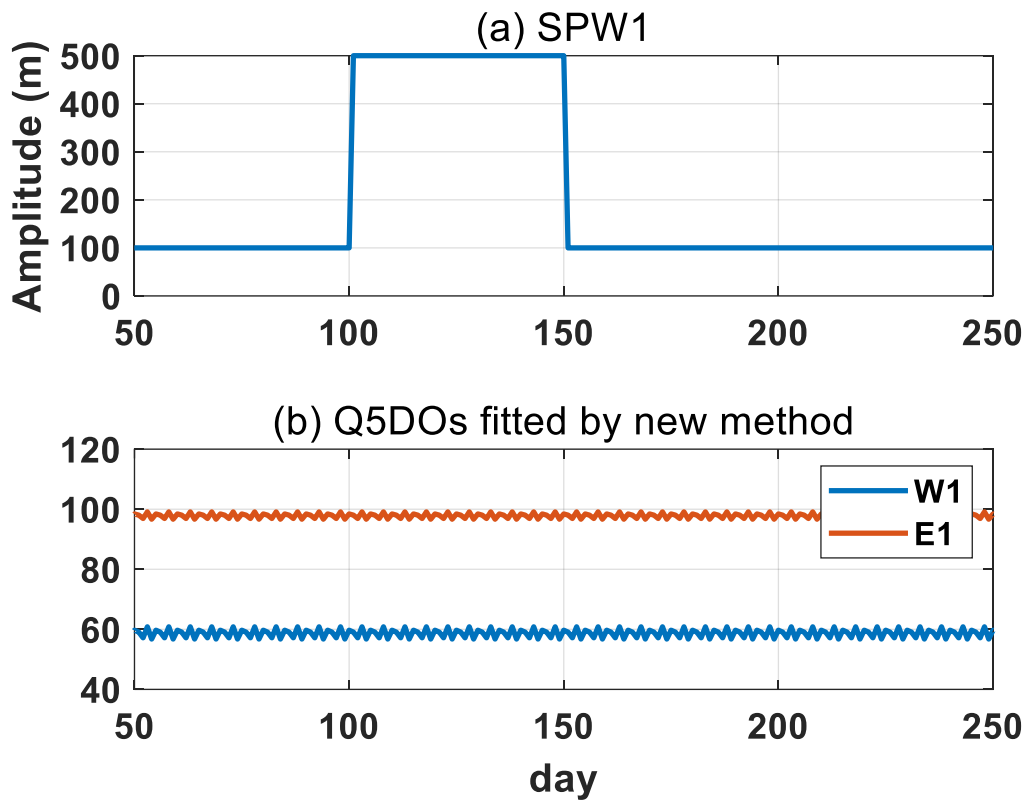
240 Then, the real amplitudes and phases of the Q5DOs (B_w , B_e , φ_w , and φ_e) can be fitted
 241 using the least-square fitting method via $Y'(x, t) = B_w \cos(\omega t + kx -$
 242 $\varphi_w) + B_e \cos(\omega t - kx - \varphi_e) + C$, where C is a constant.

243 Note that, the effect of small changes in SPWs cannot be eliminated sometimes
 244 when $\left|\frac{\partial}{\partial t} a_k(t)\right|$ are smaller than ωP . These small changes in SPWs do not have

245 significant effects on the fitted Q5DOs and their elimination depends on the phase
 246 relationships between westward and eastward Q5DOs. Nevertheless, the Monte Carlo
 247 simulations based on random phases of Q5DOs reveal that the fake fluctuations in
 248 Q5DO amplitudes due to this effect will not exceed the value of $0.1\omega P$.

249 4. Results and Discussions

250 4.1 Simulations

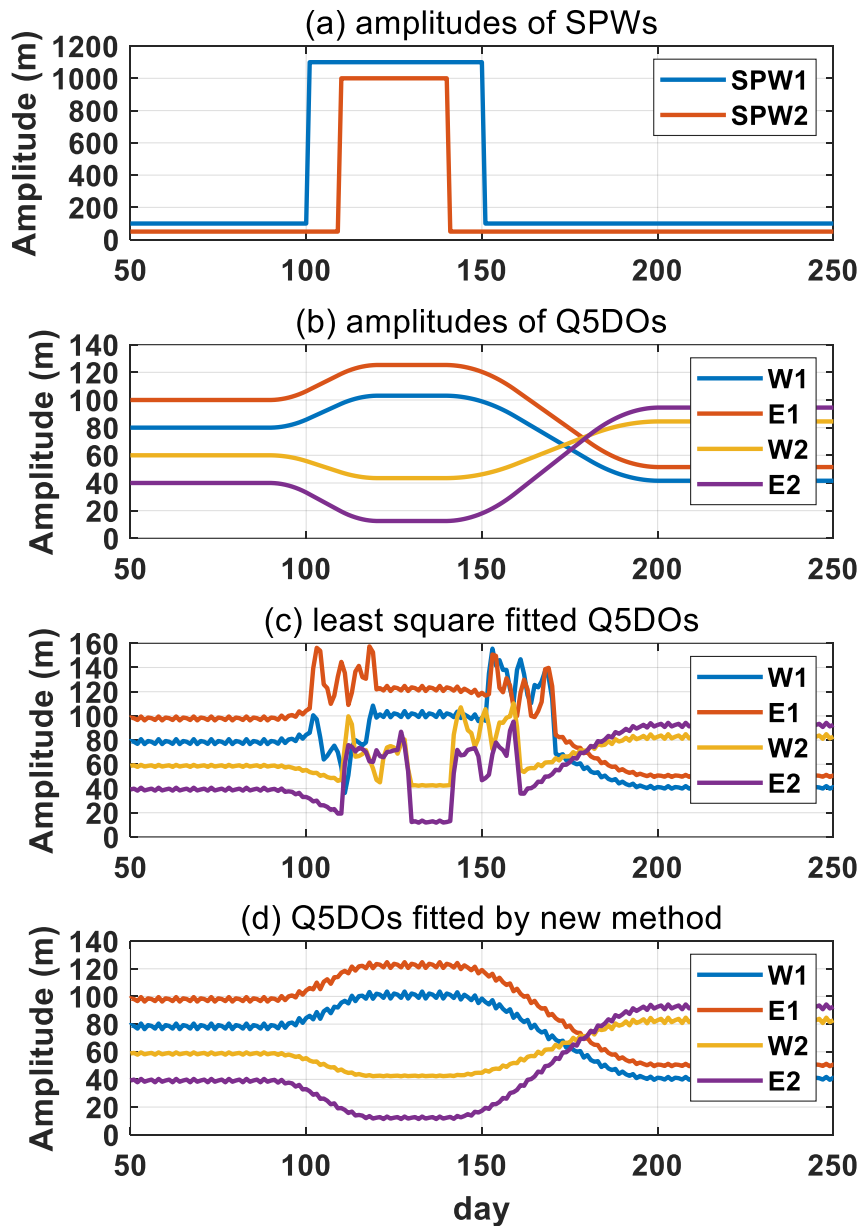


251

252 Figure 2. Simulations of the new fitting method based on synthetic data, which includes
 253 an SPW and westward and eastward Q5DOs with zonal wavenumber of 1. (a) Daily
 254 variations of the SPW amplitudes. The phase of the SPW is 0. (b) Q5DOs obtained from
 255 the new fitting method. The amplitudes are 60 m and 100 m, the phases are $-\pi/4$ and
 256 $\pi/5$ for the westward and eastward Q5DOs, respectively.

257 Based on the new fitting method, we present the fitting result in Figure 2. As shown
258 in Figure 2b, the fitted amplitudes of the Q5DOs are generally consistent with the
259 amplitudes given in the original synthetic data. The apparent fluctuations in Q5DOs
260 induced by SPWs have been removed. Note that based on the new fitting method, the
261 fitted amplitudes are not dependent on the phases of Q5DOs. The new fitting method
262 will provide the same results as those shown in Figure 2b when Q5DOs have different
263 phases (not shown). Thus, the fitted amplitudes from the new method do not rely on the
264 phase relationships of those waves. Figure 2 demonstrates that the new method is
265 effective to suppress the effect of large rapid change in SPWs, while a further
266 experiment that synthetic data containing the enhancement of both SPWs and Q5DOs
267 is needed to demonstrate that the new method can properly capture the changes of
268 Q5DOs during SSWs. Besides, we also add signals of SPWs and Q5DOs with
269 wavenumber 2 in the synthetic data to approach the real situation in satellite
270 observations. Figure 3 shows the results of the further experiment. The synthetic data
271 used in Figure 3 consist of six components: SPWs with wavenumber 1 and 2 (SPW1
272 and SPW2), westward propagating Q5DOs with wavenumber 1 and 2 (W1 and W2),
273 and eastward propagating Q5DOs with wavenumber 1 and 2 (E1 and E2). The daily
274 variation of the amplitudes for SPWs and Q5DOs are separately shown in Figures 3a
275 and 3b. The phase of SPW1, SPW2, and W1, E1, W2, and E2 Q5DOs are respectively
276 set as 0 , $\pi/6$, $-\pi/4$, $\pi/5$, $-\pi/4$, and $\pi/3$. Figures 3c and 3d present the fitting results for the
277 least-square fitting method and the new fitting method. As shown in Figure 3d, the
278 result manifests that the variations of Q5DOs can be captured based on the new method

279 and the effect of large rapid change in SPWs can be limited.



280

281 Figure 3. Simulations of the new fitting method based on synthetic data, which include

282 (a) SPW1 and SPW2 and (b) westward and eastward Q5DOs with zonal wavenumber

283 of 1 and 2. The phase of SPW1, SPW2, and W1, E1, W2, and E2 Q5DOs are

284 respectively set as 0 , $\pi/6$, $-\pi/4$, $\pi/5$, $-\pi/4$, and $\pi/3$. (c) Daily amplitudes of the fitted

285 Q5DOs obtained from the original least-square fitting method. (d) Daily amplitudes of

286 the fitted Q5DOs obtained from the new fitting method.

287 Note that some sawtooth-shaped points can be seen in the fitting results in Figures
288 1, 2, and 3. The sawtooth-shaped points are caused by removing the linear declination
289 on the time series. This process needs to be done in both original and new methods to
290 eliminate the effect of seasonal trends in the observational data on the fitting of Q5DOs.
291 The sawtooth-shaped points can be eliminated in the simulation by not removing the
292 seasonal trends, but we keep them in both original and new methods in the simulations
293 in order to be consistent with the processes in dealing with the observational data.

294 **4.2 Observations**

295 The SPWs and TPWs can be both captured in the mesosphere region and their
296 origins have been reported in some previous studies. The mesospheric SPWs are usually
297 believed to be related to the upward wave signals from the troposphere and the lower
298 stratosphere which rely on the structure of the polar vortex (e.g., Harvey et al., 2018).
299 In addition, wave-wave interactions, gravity wave forcing, and auroral heating can also
300 generate mesospheric SPWs (e.g., Lu et al., 2018; Xu et al., 2013; Smith, 2003). The
301 mesospheric TPWs are generally considered as the result of atmospheric instabilities
302 and many recent studies have noticed the relationship between extremely strong TPWs
303 and SSW events (Liu et al., 2004; Ma et al., 2020; Yamazaki et al., 2021). The
304 mesospheric TPWs during SSWs can be also secondarily generated in situ by wave-
305 wave interactions (e.g., Xiong et al., 2018; Wang et al., 2021). Nevertheless, the trigger
306 mechanisms of mesospheric TPWs are still not fully understood due to a lack of long-
307 term and high-resolution observational data in this region. Thus, satellite observations

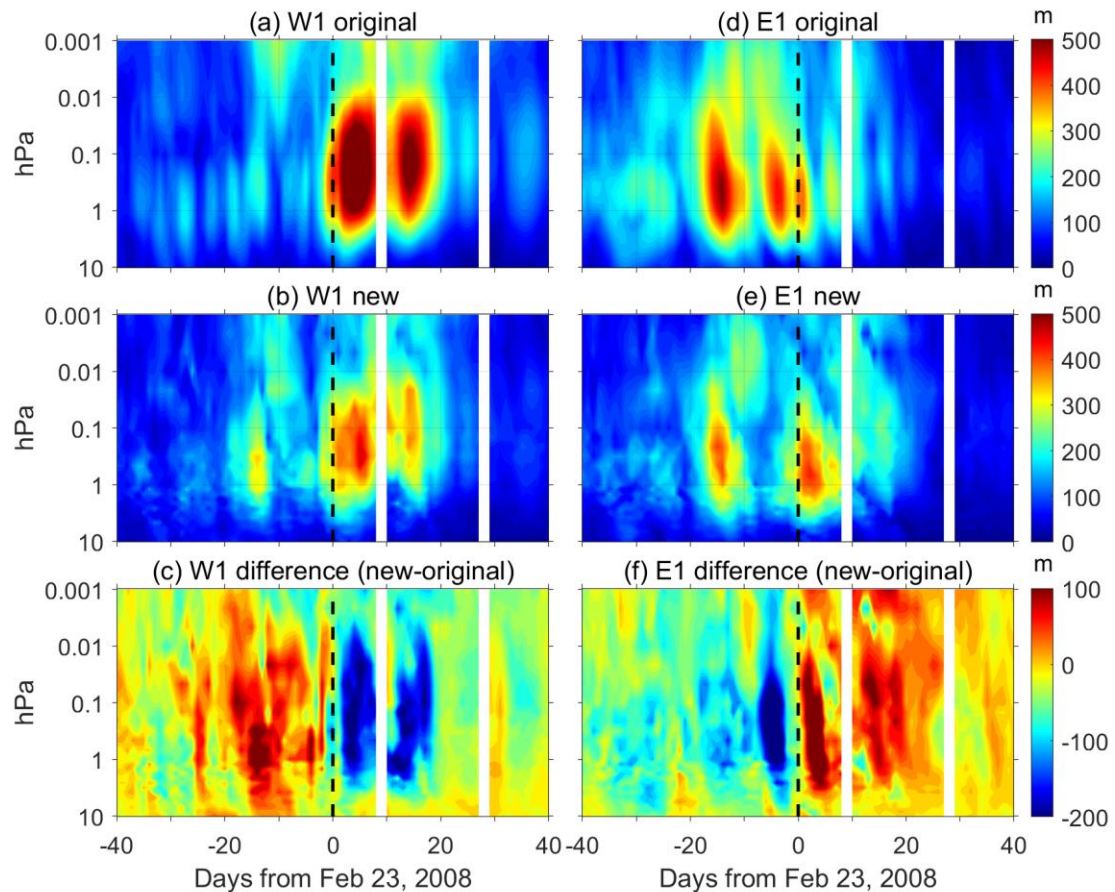
308 are widely used to reveal the feature of mesospheric TPWs. However, as indicated by
309 our simulations, the previous studies have ignored the effect of rapid and large changed
310 SPWs when calculating the variations of TPWs during SSWs. Using the geopotential
311 height data provided by the Aura/MLS measurement, we extract the variations of the
312 traveling Q5DOs at 60°N during Arctic SSWs. The effectiveness of the new fitting
313 method is discussed by comparing the results between the original least-square fitting
314 method and the new method. The daily amplitudes of the Q5DOs are obtained with the
315 largest value in the wave periods between 4 and 7 days. The fitting result is marked at
316 the end day of each 20-day window. The traveling Q5DOs with wavenumber 3 and the
317 amplitudes below 10 hPa are not shown due to their weak amplitudes. In the present
318 study, the pressure regions from 10 hPa to 1 hPa, from 1 hPa to 0.01 hPa, and from 0.01
319 hPa to 0.001 hPa are respectively discussed as the stratosphere, mesosphere, and lower
320 thermosphere.

321 Since the observation of the Aura satellite is available after August 2004, the
322 variations of traveling Q5DOs are investigated during eight mid-winter major SSWs
323 from 2005 to 2021 in the present study. Table 1 presents the eight mid-winter major
324 SSWs with their onset dates. The date with the maximum positive temperature gradient
325 between 90°N and 60°N at 10 hPa is defined as the SSW onset date, which is obtained
326 around the date of the first wind reversal during each major event (e.g., Andrews et al.,
327 1987). Note that the onset date used in the present study is only to roughly determine
328 the commencement of SSWs and our discussions are not sensitive to the non-uniformed
329 definitions of SSW onsets (e.g., Butler et al., 2015). In the present study, the SSW in

330 the winter of 2009/2010 is classified as a minor one, because the wind reversal occurred
331 18 days after the onset date. To be distinguished from the SSW in February 2018, the
332 SSW with the onset date of December 28, 2018, is discussed as the “2019 SSW” in this
333 study. The SSWs before 2013 have been widely studied in previous studies (e.g., Choi
334 et al., 2019; Charlton and Polvani, 2007; Butler et al., 2017; Liu et al., 2019; Rao et al.,
335 2019), details of the three major SSWs from 2018 to 2021 can be referred to many
336 recent reports (e.g., Rao et al., 2018, 2020, 2021; Wang et al., 2019; Davis et al., 2022;
337 Okui et al., 2021; Wright et al., 2021).

338 Table 1. Mid-winter major SSWs from 2005 to 2021.

SSW	Onset Date	First Wind Reversal Date
2006	January 22, 2006	January 21, 2006
2007	February 24, 2007	February 24, 2007
2008	February 23, 2008	February 22, 2008
2009	January 23, 2009	January 24, 2009
2013	January 6, 2013	January 6, 2013
2018	February 11, 2018	February 12, 2018
2019	December 28, 2018	January 2, 2019
2021	January 4, 2021	January 5, 2021

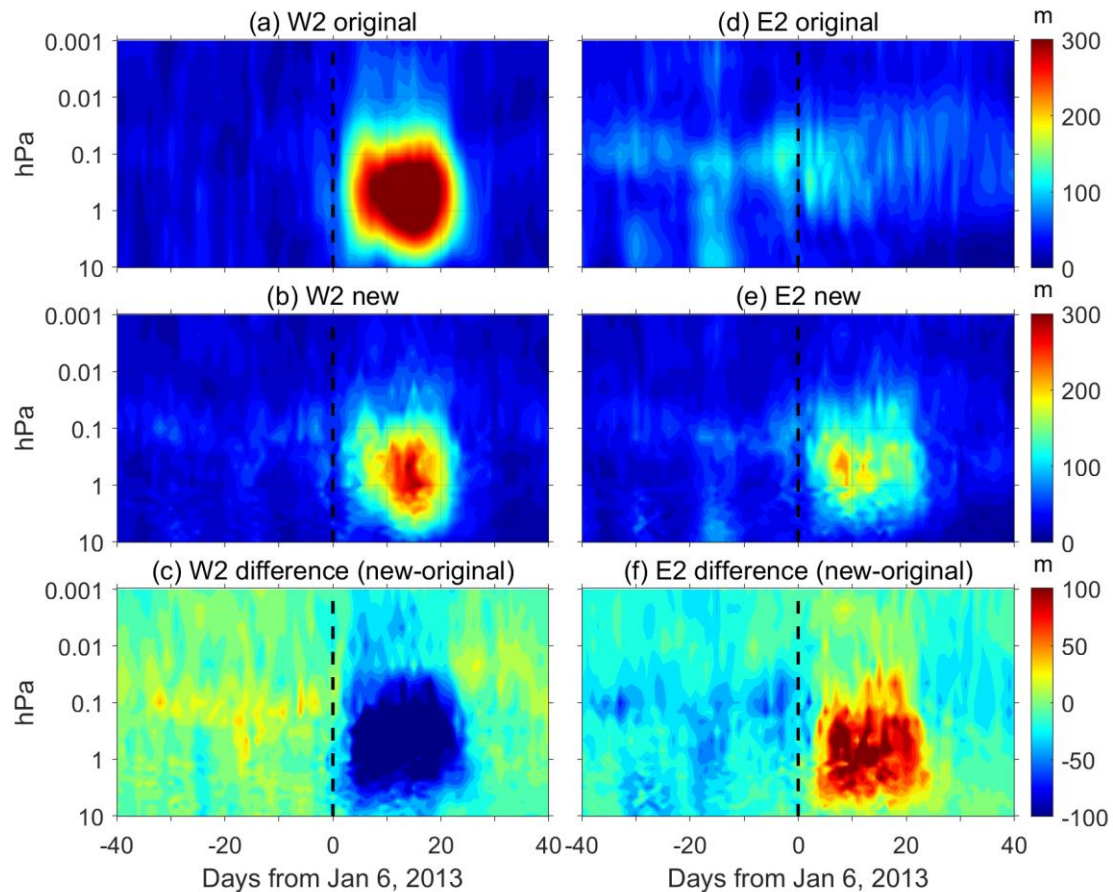


339

340 Figure 4. The amplitudes of W1 (left column) and E1 (right column) Q5DOs during the
 341 2008 SSW obtained by the original least-square fitting method (top row) and the new
 342 fitting method (middle row). The differences between the new and original methods are
 343 shown in the bottom row (c and f). Contour steps are 10 m.

344 Comparisons of fitted amplitudes of traveling Q5DOs are first shown in Figures 4
 345 and 5, respectively for wavenumber 1 during the 2008 SSW and wavenumber 2 during
 346 the 2013 SSW. Results for each case are given in 81 days, which is from 40 days before
 347 to 40 days after the SSW onset date (day 0). Figure 4 presents the amplitudes of W1
 348 and E1 Q5DOs obtained from both original (top) and new (middle) methods during the
 349 2008 SSW. The differences are calculated by subtracting the fitting result of the original
 350 method from the new method, which are given at the bottom of Figure 4. Amplitudes

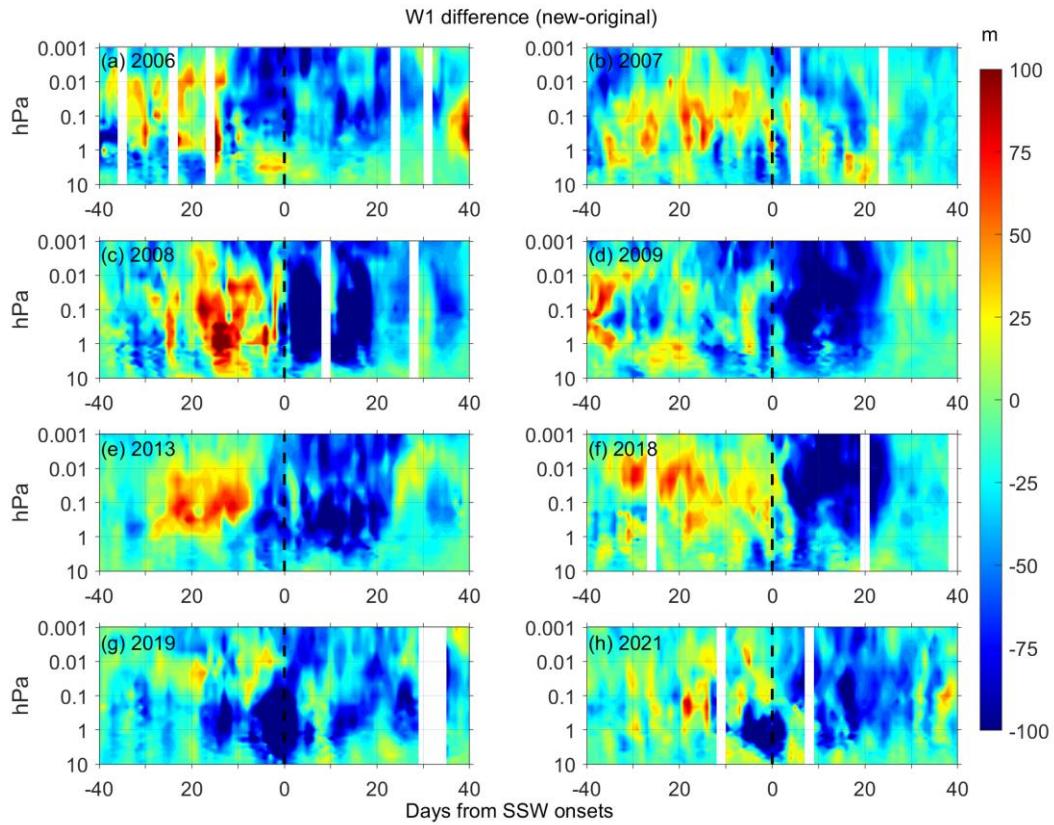
351 are not fitted in the white area where the available data are less than 60% in each
352 window. As shown in Figure 4a, the W1 Q5DOs fitted by the original least-square
353 fitting method reveal a significant response to the onset of 2008 SSW. The amplitudes
354 of the W1 Q5DOs in the mesosphere are larger than 500 m from day 0 to day 20 with
355 a maximum amplitude of 628 m on day 5. Figure 4b suggests that the amplitudes
356 obtained from the new method are lower than 500 m during the 2008 SSW. The
357 maximum amplitude obtained from the new method is 466 m on day 5, which is about
358 75% of the amplitude obtained from the original least-square fitting method. The
359 negative differences shown in Figure 4c are generally larger than 200 m from day 0 to
360 day 20 in the mesosphere, which indicates that the amplitudes of W1 Q5DOs after the
361 onset of 2008 SSW might be overestimated by the original least-square fitting method.
362 Nevertheless, positive differences larger than 100 m are also captured before the SSW
363 onset (day -15) around 1 hPa as shown in Figure 4c, which reveals that the amplitudes
364 of W1 Q5DOs obtained from the original method can be also underestimated during
365 the 2008 SSW. For the amplitudes of E1 Q5DOs during the 2008 SSW, the original
366 least-square fitting method may have an overestimation before the onset date and an
367 underestimation after the onset date. As shown in Figure 4f, the positive and negative
368 differences both have maximum amplitudes over 200 m in the mesosphere around the
369 onset date.



370

371 Figure 5. Same as Figure 4 but for W2 and E2 Q5DOs during the 2013 SSW.

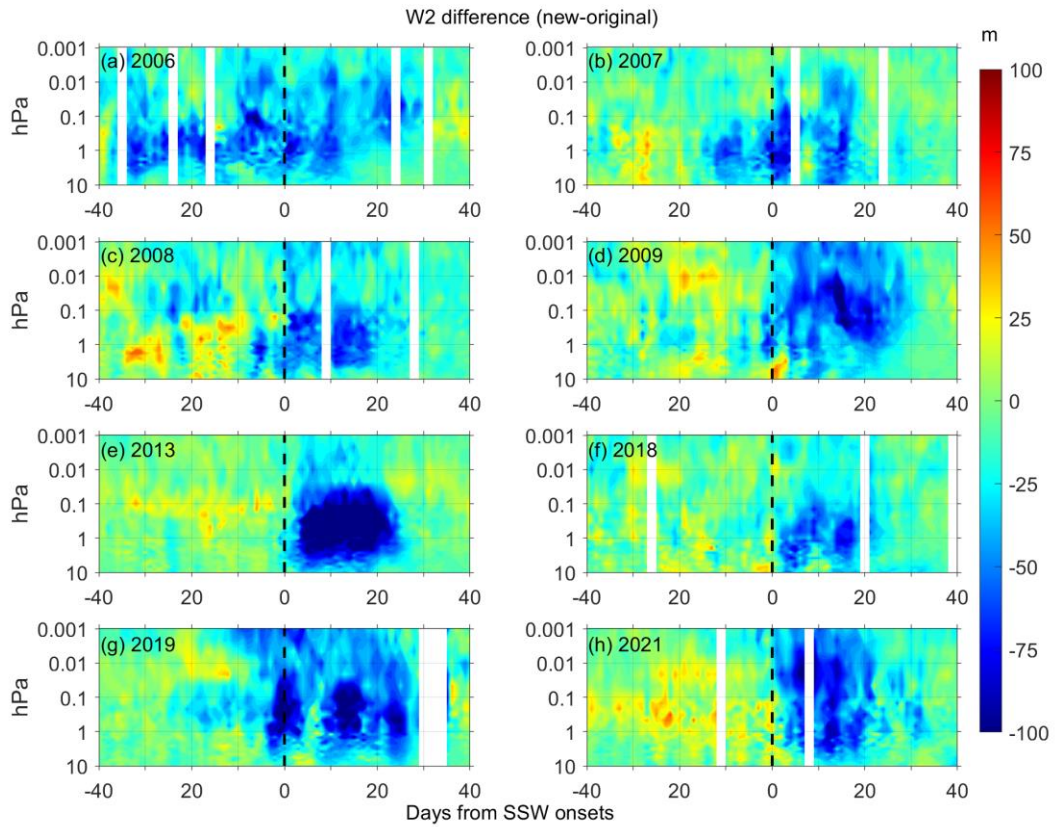
372 Figure 5 presents the same results as Figure 4 but for the amplitudes of W2 and
 373 E2 Q5DOs during the 2013 SSW. As shown in Figure 5, strong enhancements of W2
 374 Q5DOs and weak amplitudes of E2 Q5DOs after the 2013 SSW are captured by the
 375 original least-square fitting method. However, results from the new method after the
 376 onset of 2013 SSW suggest that based on the original least-square fitting method, the
 377 amplitudes of W2 Q5DOs might be overestimated and the amplitudes of E2 Q5DOs
 378 may be underestimated. The maximum positive and negative differences are both over
 379 100 m. In order to understand the common differences between the two methods, we
 380 calculate the differences during the eight SSWs and present the results in Figures 6, 7,
 381 8, and 9 for the W1, W2, E1, and E2 components, respectively.



382

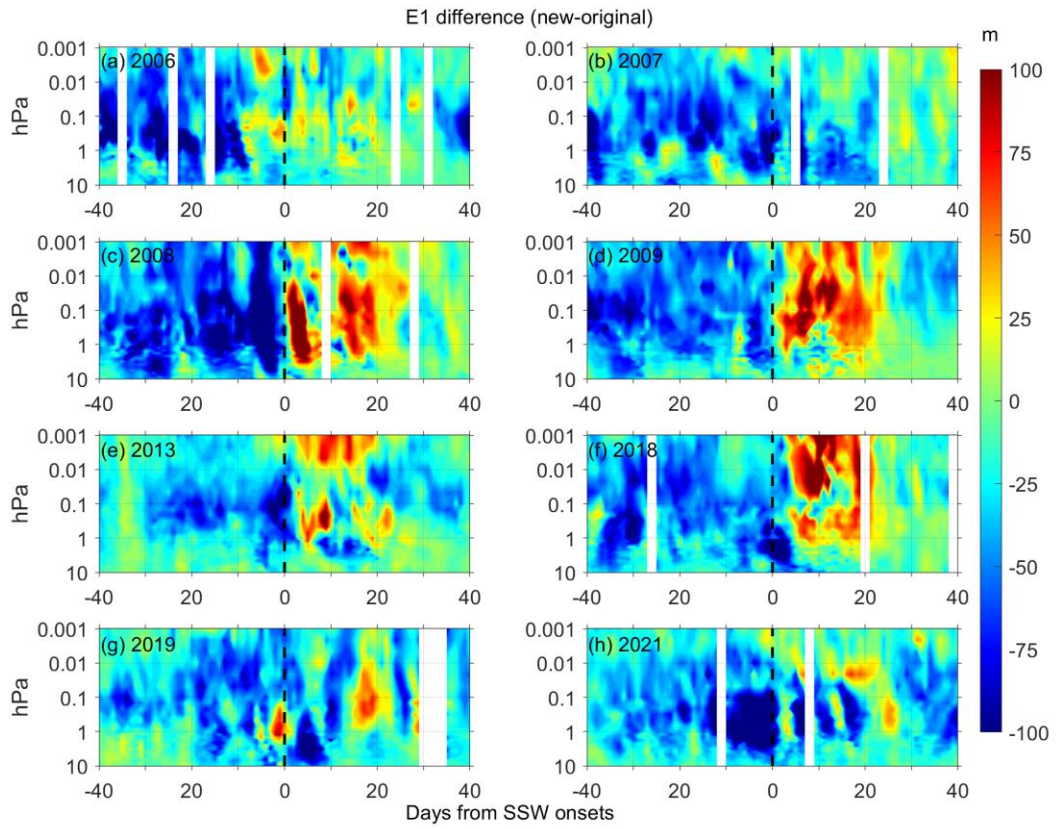
383 Figure 6. The differences in the fitted W1 Q5DO amplitudes between the new and

384 original methods during 8 major SSWs since 2006 (from a to h). Contour steps are 5 m.



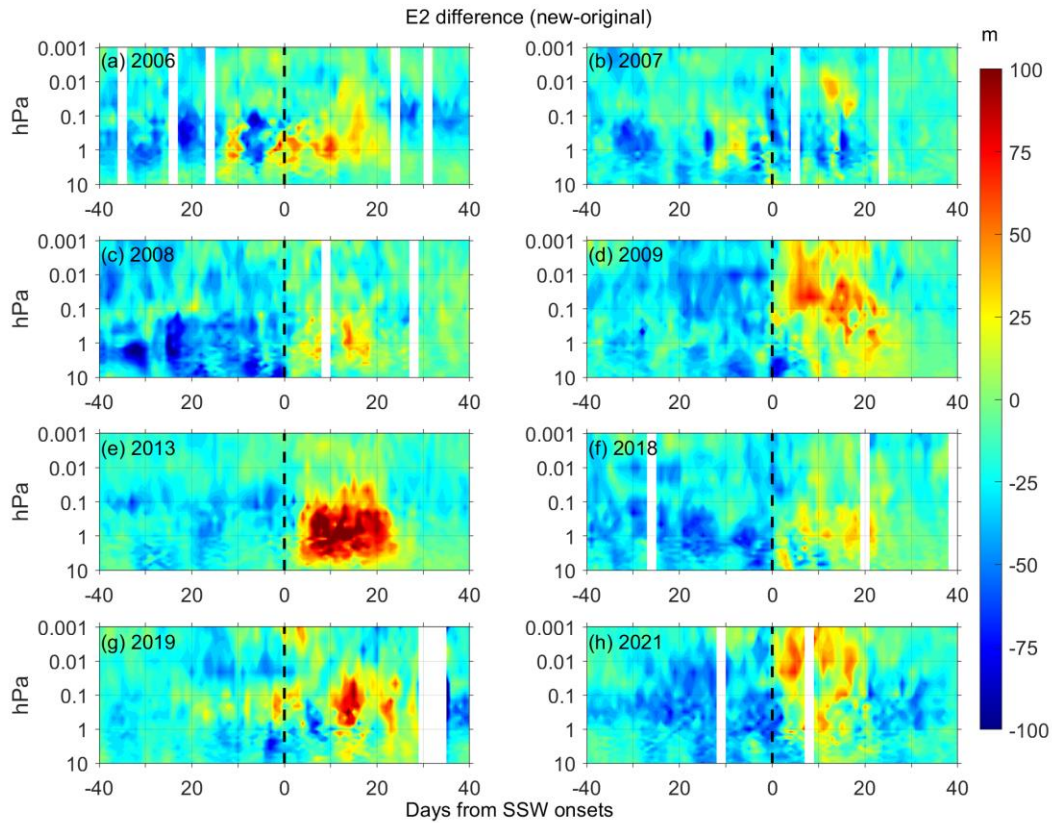
385

386 Figure 7. Same as Figure 6 but for the W2 component.



387

388 Figure 8. Same as Figure 6 but for the E1 component.



389

390 Figure 9. Same as Figure 6 but for the E2 component.

391 As shown in Figures 6 and 7, the difference in the fitted westward propagating
 392 Q5DO amplitudes between the new and original methods are usually negative after the
 393 SSW onsets, which suggests that the amplitudes of the westward propagating Q5DOs
 394 might be overestimated by the original least-square fitting method after the SSW onsets.
 395 However, the difference in the fitted eastward propagating Q5DO amplitudes between
 396 the new and original methods (as shown in Figures 8 and 9) are usually positive after
 397 the SSW onsets, which indicates that the amplitudes of the eastward propagating
 398 Q5DOs might be underestimated by the original least-square fitting method after the
 399 SSW onsets. Additionally, the E1 Q5DOs before the SSW onsets might be also
 400 overestimated by the original least-square fitting method as seen in Figure 8. The

401 enhancements of traveling Q5DOs during SSWs reported in previous studies are
402 usually westward propagating after the SSW onsets and eastward propagating before
403 the SSW onsets (e.g., Gong et al., 2018; Yu et al., 2022). Thus, our analyses indicate
404 that the previously-reported Q5DOs obtained by satellite measurements during SSWs
405 might be contaminated by SPWs. The amplitudes of the enhancement of Q5DOs during
406 SSWs might be overestimated. Additionally, the westward propagating Q5DOs before
407 the SSW onsets and the eastward propagating Q5DOs after the SSW onsets might be
408 underestimated by the original least-square fitting method. Therefore, in future studies
409 of the activities of Q5DOs during SSWs based on satellite observations and reanalysis
410 data, the variations of different wave components in Q5DOs have to be carefully
411 derived by eliminating the effects of SPWs.

412 Generally, the TPWs, including the Q5DOs, dominate in the mesosphere and
413 lower thermosphere, which are enhanced seasonally during winter and spring times and
414 largely control the neutral winds and temperatures in the middle atmosphere (e.g., Gong
415 et al., 2018, 2019; Pancheva et al., 2018; Yamazaki et al., 2020, 2021). The vertical and
416 latitudinal propagation of the TPWs can also transport energies and lead to couplings
417 on a global scale (e.g., Koushik et al., 2020; Ma et al., 2022). Thus, extracting the real
418 amplitudes of the traveling waves is also important to reveal the characteristics in the
419 mesosphere and the vertical couplings in the middle atmosphere. Some extremely
420 strong TPWs are found to be related to the occurrence of SSWs, but their trigger
421 mechanisms have not been fully understood (e.g., Ma et al., 2020; Yamazaki et al.,
422 2021). However, the rapid and large change of the SPWs during SSWs can lead to

423 contaminations when deriving the real amplitudes of TPWs based on satellite
424 observations or reanalysis data. The new method proposed in the present study can
425 capture a more accurate variation in the amplitudes of TPWs than the old one. The new
426 method is based on the examinations during SSWs due to the assumption that a rapid
427 and large change in SPWs is usually observed during SSWs. Nevertheless, the new
428 method can also be used to extract the amplitudes of TPWs in the mesosphere during
429 other seasons and cases, such as the spring final warmings and other disturbances in
430 stratospheric vortices. Based on the new method, the common feature of the TPWs
431 revealed by satellite observations in the mesosphere and lower thermosphere can be
432 reevaluated, and the trigger mechanism of the mesospheric TPWs during SSWs can be
433 further understood.

434 **5. Summary and conclusions**

435 In the present study, a new fitting method is developed to derive the variations of
436 traveling quasi-5-day waves (Q5DOs) by inhibiting the effect of rapid and large
437 changes in the amplitudes of stationary planetary waves (SPWs). The effectiveness of
438 the new method is demonstrated by both synthetic and observational data. According
439 to the simulations, the new method can capture the variations of the amplitudes of
440 traveling Q5DOs when large and rapid changes in SPWs are given. Based on the
441 geopotential height data measured by MLS onboard the Aura satellite, we compare the
442 difference of the traveling Q5DOs amplitudes between the original least-square fitting
443 method and the new fitting method in the middle atmosphere during eight Arctic major

444 SSWs from 2005 to 2021. Our results indicate that the enhancements of traveling
445 Q5DOs during SSWs reported in previous studies might be overestimated due to
446 ignoring the effect of large rapid changes in SPWs. Besides, the amplitudes of westward
447 propagating Q5DOs before the SSW onsets and the amplitudes of eastward propagating
448 Q5DOs after the SSW onsets might be underestimated. Note that since the amplitudes
449 of SPWs cannot be derived accurately due to the aliasing of Q5DOs, the contribution
450 of the SPWs and Q5DOs during SSWs cannot be quantified in the present method. Our
451 goal is to attenuate the effect of SPWs on the derivation of Q5DOs during SSWs.
452 Future works are needed to examine the effectiveness of the new method by using
453 traveling planetary oscillations with other periods, such as the quasi-10-day and quasi-
454 16-day waves.

455

456 **Data availability.** The Aura/MLS geopotential height data can be downloaded through
457 the Goddard Earth Sciences Data and Information Services Center via
458 (https://acdisc.gesdisc.eosdis.nasa.gov/data/Aura_MLS_Level2/ML2GPH.004/).

459

460 **Author contributions.** ZM and YG proposed the scientific ideas. QX and ZM
461 contributed to data processing and simulation programming. ZM, YG, and SZ
462 completed the analysis and manuscript. CH and KH discussed the results in the
463 manuscript.

464

465 **Competing interests.** The authors declare that they have no conflict of interest.

466

467

468 **Acknowledgments.** We acknowledge the Goddard Earth Sciences Data and
469 Information Services Center for providing the Aura/MLS geopotential height data.

470

471 **Financial support.** This study is supported by the National Natural Science Foundation
472 of China (through grants 42104145 and 41574142), the Fundamental Research Funds
473 for the Central Universities 2042021kf0021, and the China Postdoctoral Science
474 Foundation (through grants 2021M692465 and 2020TQ0230).

475

476

477 **References**

478 Andrews, D. G., Holton, J. R., and Leovy, C. B.: Middle Atmosphere Dynamics, 1st
479 ed., Academic Press, San Diego, Calif, 1987.

480 Baldwin, M. P., Ayarzagüena, B., Birner, T., Butchart, N., Butler, A. H., and Charlton-
481 Perez, A. J.: Sudden stratospheric warmings. *Reviews of Geophysics*, 58,
482 e2020RG000708. <https://doi.org/10.1029/2020RG000708>, 2021.

483 Butler, A. H., Seidel, D. J., Hardiman, S. C., Butchart, N., Birner, T., and Match, A.:
484 Defining Sudden Stratospheric Warmings, *Bulletin of the American*
485 *Meteorological Society*, 96(11), 1913-1928, [https://doi.org/10.1175/BAMS-D-13-](https://doi.org/10.1175/BAMS-D-13-00173.1)
486 [00173.1](https://doi.org/10.1175/BAMS-D-13-00173.1), 2015.

487 Butler, A. H., Sjoberg, J. P., Seidel, D. J., and Rosenlof, K. H.: A sudden stratospheric
488 warming compendium. *Earth System Science Data*, 9, 63–76.
489 <https://doi.org/10.5194/essd-9-63-2017>, 2017.

490 Charlton, A. J., and Polvani, L. M.: A new look at stratospheric sudden warmings. Part
491 I: Climatology and modeling benchmarks. *J. Climate*, 20(3), 449–469.
492 <https://doi.org/10.1175/JCLI3996.1>, 2007.

493 Choi, H., Kim, B. M., and Choi, W.: Type classification of sudden stratospheric
494 warming based on pre- and postwarming periods. *Journal of Climate*, 32(8), 2349–
495 2367. <https://doi.org/10.1175/JCLI-D-18-0223.1>, 2019

496 Davis, N.A., Richter, J.H., Glanville, A.A., Edwards, J., and LaJoie, E.: Limited surface
497 impacts of the January 2021 sudden stratospheric warming. *Nature*
498 *Communications*, 13, 1136. <https://doi.org/10.1038/s41467-022-28836-1>, 2022.

499 Domeisen, D. I. V., Butler, A. H., Charlton-Perez, A. J., Ayarzagüena, B., Baldwin, M.
500 P., Dunn-Sigouin, E., Furtado, J. C., Garfinkel, C. I., Hitchcock, P., Karpechko, A.
501 Yu., Kim, H., Knight, J., Lang, A. L., Lim, E., Marshall, A., Roff, G., Schwartz,
502 C., Simpson, I. R., Son, S., Taguchi, M.: The role of the stratosphere in subseasonal
503 to seasonal prediction: 2. Predictability arising from stratosphere-troposphere
504 coupling. *Journal of Geophysical Research: Atmospheres*, 125, e2019JD030923.
505 <https://doi.org/10.1029/2019JD030923>, 2020.

506 Gong, Y., Li, C., Ma, Z., Zhang, S., Zhou, Q., Huang, C., Huang, K., Li, G., Ning, B.:
507 Study of the quasi-5-day wave in the MLT region by a meteor radar chain. *Journal*

508 of Geophysical Research: Atmospheres, 123, 9474–9487.

509 <https://doi.org/10.1029/2018JD029355>, 2018.

510 Gong, Y., Wang, H., Ma, Z., Zhang, S., Zhou, Q., Huang, C., and Huang, K.: A statistical
511 analysis of the propagating quasi 16-day waves at high latitudes and their response
512 to sudden stratospheric warmings from 2005 to 2018. Journal of Geophysical
513 Research: Atmospheres, 124, 12,617–12,630. <https://doi.org/10.1029/2019JD031482>,
514 2019.

515 Harada, Y., and Hirooka, T.: Extraordinary features of the planetary wave propagation
516 during the boreal winter 2013/2014 and the zonal wave number two predominance.
517 Journal of Geophysical Research: Atmospheres, 122(21), 11374–11387.
518 <https://doi.org/10.1002/2017JD027053>, 2017.

519 Harvey, V. L., Randall, C. E., Goncharenko, L., Becker, E., and France, J.: On the
520 upward extension of the polar vortices into the mesosphere. Journal of
521 Geophysical Research: Atmospheres, 123(17), 9171–9191.
522 <https://doi.org/10.1029/2018JD028815>, 2018.

523 Huang, Y. Y., Zhang, S., Li, C. Y., Li, H. J., Huang, K., and Huang, C.: Annual and inter-
524 annual variations in global 6.5DWs from 20–110 km during 2002–2016 observed
525 by TIMED/SABER. Journal of Geophysical Research: Space Physics, 122, 8985–
526 9002. <https://doi.org/10.1002/2017JA023886>, 2017.

527 King, A. D., Butler, A. H., Jucker, M., Earl, N. O., and Rudeva, I.: Observed
528 relationships between sudden stratospheric warmings and European climate

529 extremes. *Journal of Geophysical Research: Atmospheres*, 124(24), 13943–13961.
530 <https://doi.org/10.1029/2019JD030480>, 2019.

531 Koushik, N., Kumar, K. K., Ramkumar, G., Subrehmanyam, K. V., Kishore Kumar, G.,
532 Hocking, W. K., He, M., Latteck, R.: Planetary waves in the mesosphere lower
533 thermosphere during stratospheric sudden warming: Observations using a network
534 of meteor radars from high to equatorial latitudes. *Climate Dynamics*, 54(9–10),
535 4059–4074. <https://doi.org/10.1007/s00382-020-05214-5>, 2020.

536 Kozubek, M., Krizan, P., and Lastovicka, J.: Northern Hemisphere stratospheric winds
537 in higher midlatitudes: longitudinal distribution and long-term trends. *Atmos.*
538 *Chem. Phys.*, 15(4), 2203–2213. <https://doi.org/10.5194/acp-15-2203-2015>, 2015.

539 Lawrence, Z. D., and Manney, G. L.: Characterizing stratospheric polar vortex
540 variability with computer vision techniques. *Journal of Geophysical Research:*
541 *Atmospheres*, 123(3), 1510–1535., 2018.

542 Lin, J. T., Lin, C. H., Rajesh, P. K., Yue, J., Lin, C. Y., and Matsuo, T.: Local-time and
543 vertical characteristics of quasi-6-day oscillation in the ionosphere during the 2019
544 Antarctic sudden stratospheric warming. *Geophysical Research Letters*, 47.
545 <https://doi.org/10.1029/2020GL090345>, 2020.

546 Livesey, N. J., Read, W. G., Wagner, P. A., Froidevaux, L., Lambert, A., Manney, G. L.,
547 Millan Valle, L. F., Pumphrey, H. C., Santee, M. L., Schwartz, M. J., Wang, S.,
548 Fuller, R. A., Jarnot, R. F., Knosp, B. W., and Martinez, E.: Earth Observing
549 System (EOS) Aura Microwave Limb Sounder (MLS) Version 4.2x Level 2 data

550 quality and description document, Tech. Rep. D-33509 Rev. A, JPL, 2015.

551 Liu, H. L., Talaat, E. R., Roble, R. G., Lieberman, R. S., Riggin, D. M., and Yee, J. H.:
552 The 6.5-day wave and its seasonal variability in the middle and upper atmosphere.
553 Journal of Geophysical Research, 109, D21112. <https://doi.org/10.1029/2004JD004795>,
554 2004.

555 Liu, S.-M., Chen, Y.-H., Rao, J., Cao, C., Li, S.-Y., Ma, M.-H., and Wang, Y.-B.: Parallel
556 Comparison of Major Sudden Stratospheric Warming Events in CESM1-WACCM
557 and CESM2-WACCM. Atmosphere, 10, 679. <https://doi.org/10.3390/atmos10110679>,
558 2019.

559 Longuet-Higgins, M. S.: The eigenfunctions of Laplace's tidal equations over a sphere,
560 Philosophical Transactions of the Royal Society of London. 262, 511-607.
561 doi:10.1098/rsta.1968.0003, 1968.

562 Lu, X., Wu, H., Oberheide, J., Liu, H.-L., and McNerney, J. M.: Latitudinal double-
563 peak structure of stationary planetary wave 1 in the austral winter middle
564 atmosphere and its possible generation mechanism. Journal of Geophysical
565 Research: Atmospheres, 123, 11,551–11,568.
566 <https://doi.org/10.1029/2018JD029172>, 2018.

567 Ma, Z., Gong, Y., Zhang, S., Zhou, Q., Huang, C., Huang, K., Luo, J., Yu, Y., Li, G.:
568 Study of a quasi-4-day oscillation during the 2018/2019 SSW over Mohe, China.
569 Journal of Geophysical Research: Space Physics, 125, e2019JA027687.
570 <https://doi.org/10.1029/2019JA027687>, 2020.

571 Ma, Z., Gong, Y., Zhang, S., Xiao, Q., Xue, J., Huang, C., and Huang, K.:
572 Understanding the excitation of quasi-6-day waves in both hemispheres during the
573 September 2019 Antarctic SSW. *Journal of Geophysical Research: Atmospheres*,
574 127, e2021JD035984. <https://doi.org/10.1029/2021JD035984>, 2022.

575 Manney, G. L., Schwartz, M. J., Krüger, K., Santee, M. L., Pawson, S., Lee, J. N., Daffer,
576 W. H., Fuller, R. A., and Livesey, N. J.: Aura Microwave Limb Sounder
577 observations of dynamics and transport during the record breaking 2009 Arctic
578 stratospheric major warming. *Geophys. Res. Lett.*, 36(12), L12815.
579 <https://doi.org/10.1029/2009GL038586>, 2009.

580 Matsuno, T.: A dynamical model of the stratospheric sudden warming. *Journal of the*
581 *Atmospheric Sciences*, 28, 1479–1494. [https://doi.org/10.1175/1520-](https://doi.org/10.1175/1520-0469(1971)028<1479:ADMOTS>2.0.CO;2)
582 [0469\(1971\)028<1479:ADMOTS>2.0.CO;2](https://doi.org/10.1175/1520-0469(1971)028<1479:ADMOTS>2.0.CO;2), 1971.

583 Okui, H., Sato, K., Koshin, D., and Watanabe, S.: Formation of a mesospheric inversion
584 layer and the subsequent elevated stratopause associated with the major
585 stratospheric sudden warming in 2018/19. *Journal of Geophysical Research:*
586 *Atmospheres*, 126, e2021JD034681. <https://doi.org/10.1029/2021JD034681>, 2021.

587 Pancheva, D., Mukhtarov, P., and Siskind, D. E.: The quasi-6-day waves in NOGAPS-
588 ALPHA forecast model and their climatology in MLS/Aura measurements (2005-
589 2014), *Journal of Atmospheric and Solar-Terrestrial Physics*, 181, 19-37,
590 <https://doi.org/10.1016/j.jastp.2018.10.008>, 2018.

591 Qin, Y., Gu, S-Y., Teng, C-K-M., Dou, X-K., Yu, Y., and Li, N.: Comprehensive study

592 of the climatology of the quasi-6-day wave in the MLT region based on aura/MLS
593 observations and SDWACCM-X simulations. *Journal of Geophysical Research:*
594 *Space Physics*, 126, e2020JA028454. <https://doi.org/10.1029/2020JA028454>, 2021.

595 Rao, J., Ren, R., Chen, H., Liu, X., Yu, Y., Hu, J., and Zhou, Y.: Predictability of
596 stratospheric sudden warmings in the Beijing Climate Center Forecast System
597 with statistical error corrections. *Journal of Geophysical Research:*
598 *Atmospheres*, 124, 8385–8400. <https://doi.org/10.1029/2019JD030900>, 2019.

599 Rao, J., Garfinkel, C. I., and White, I. P.: Predicting the downward and surface influence
600 of the February 2018 and January 2019 sudden stratospheric warming events in
601 subseasonal to seasonal (S2S) models. *Journal of Geophysical Research:*
602 *Atmospheres*, 125, e2019JD031919. <https://doi.org/10.1029/2019JD031919>, 2020.

603 Rao, J., Ren, R., Chen, H., Yu, Y., and Zhou, Y.: The stratospheric sudden warming
604 event in February 2018 and its prediction by a climate system model. *Journal of*
605 *Geophysical Research: Atmospheres*, 123, 13,332–13,345.
606 <https://doi.org/10.1029/2018JD028908>, 2018.

607 Rao, J., Garfinkel, C. I., Wu, T., Lu, Y., Lu, Q., and Liang, Z.: The January 2021 sudden
608 stratospheric warming and its prediction in subseasonal to seasonal models.
609 *Journal of Geophysical Research: Atmospheres*, 126, e2021JD035057.
610 <https://doi.org/10.1029/2021JD035057>, 2021.

611 Rhodes, C. T., Limpasuvan, V., and Orsolini, Y. J.: Eastward-propagating planetary
612 waves prior to the January 2009 sudden stratospheric warming. *Journal of*

613 Geophysical Research: Atmospheres, 126, e2020JD033696.
614 <https://doi.org/10.1029/2020JD033696>, 2021.

615 Seviour, W. J. M., Mitchell, D. M., and Gray, L. J.: A practical method to identify
616 displaced and split stratospheric polar vortex events. *Geophys. Res. Lett.*, 40(19),
617 5268–5273. <https://doi.org/10.1002/grl.50927>, 2013.

618 Smith, A. K.: The origin of stationary planetary waves in the upper mesosphere. *Journal*
619 *of the Atmospheric Sciences*, 60(24), 3033–3041. [https://doi.org/10.1175/1520-](https://doi.org/10.1175/1520-0469(2003)060<3033:TOOSPW>2.0.CO;2)
620 [0469\(2003\)060<3033:TOOSPW>2.0.CO;2](https://doi.org/10.1175/1520-0469(2003)060<3033:TOOSPW>2.0.CO;2), 2003.

621 Tunbridge, V. M., Sandford, D. J., and Mitchell, N. J.: Zonal wave numbers of the
622 summertime 2 day planetary wave observed in the mesosphere by EOS Aura
623 Microwave Limb Sounder, *J. Geophys. Res.*, 116, D11103,
624 doi:10.1029/2010JD014567, 2011.

625 Wang, J. C., Palo, S. E., Forbes, J. M., Marino, J., Moffat-Griffin, T., and Mitchell, N.
626 J.: Unusual quasi 10-day planetary wave activity and the ionospheric response
627 during the 2019 Southern Hemisphere sudden stratospheric warming. *Journal of*
628 *Geophysical Research: Space Physics*, 126, e2021JA029286.
629 <https://doi.org/10.1029/2021JA029286>, 2021.

630 Wang, Y., Shulga, V., Milinevsky, G., Patoka, A., Evtushevsky, O., Klekociuk, A., Han,
631 W., Grytsai, A., Shulga, D., Myshenko, V., and Antyufeyev, O.: Winter 2018 major
632 sudden stratospheric warming impact on midlatitude mesosphere from microwave
633 radiometer measurements, *Atmos. Chem. Phys.*, 19, 10303–10317,

634 <https://doi.org/10.5194/acp-19-10303-2019>, 2019.

635 White, I. P., Garfinkel, C. I., Cohen, J., Jucker, M., and Rao, J.: The impact of split and
636 displacement sudden stratospheric warmings on the troposphere. *Journal of*
637 *Geophysical Research: Atmospheres*, 126, e2020JD033989.
638 <https://doi.org/10.1029/2020JD033989>, 2021.

639 Wright, C. J., Hall, R. J., Banyard, T. P., Hindley, N. P., Krisch, I., Mitchell, D. M., and
640 Seviour, W. J. M.: Dynamical and surface impacts of the January 2021 sudden
641 stratospheric warming in novel Aeolus wind observations, MLS and ERA5,
642 *Weather Clim. Dynam.*, 2, 1283–1301, <https://doi.org/10.5194/wcd-2-1283-2021>,
643 2021.

644 Wu, D. L., Hays, P. B., and Skinner, W. R.: A least-squares method for spectral-analysis
645 of space-time series, *J. Atmos. Sci.*, 52, 3501–3511, [https://doi.org/10.1175/1520-0469\(1995\)052<3501:ALSMFS>2.0.CO;2](https://doi.org/10.1175/1520-0469(1995)052<3501:ALSMFS>2.0.CO;2), 1995.

647 Xiong, J., Wan, W., Ding, F., Liu, L., Hu, L., and Yan, C.: Two day wave traveling
648 westward with wave number 1 during the sudden stratospheric warming in January
649 2017. *Journal of Geophysical Research: Space Physics*, 123, 3005–3013.
650 <https://doi.org/10.1002/2017JA02517>, 2018.

651 Xu, J., Smith, A. K., Wang, W., Jiang, G., Yuan, W., Gao, H., Yue, J., Funke, B., López-
652 Puertas, M., Russell, I. I. I., and M, J.: An observational and theoretical study of
653 the longitudinal variation in neutral temperature induced by aurora heating in the
654 lower thermosphere. *Journal of Geophysical Research: Space Physics*, 118, 7410–

655 7425, 2013.

656 Yamazaki, Y., and Matthias, V.: Large-amplitude quasi-10-day waves in the middle
657 atmosphere during final warmings. *Journal of Geophysical Research:*
658 *Atmospheres*, 124, 9874–9892. <https://doi.org/10.1029/2019JD030634>, 2019.

659 Yamazaki, Y., Matthias, V., Miyoshi, Y., Stolle, C., Siddiqui, T., Kervalishvili, G.,
660 Laštovička, J., Kozubek, M., Ward, W., Themens, D. R., Kristoffersen, S., Alken,
661 P.: September 2019 Antarctic sudden stratospheric warming: Quasi-6-day wave
662 burst and ionospheric effects. *Geophysical Research Letters*, 47, e2019GL086577.
663 <https://doi.org/10.1029/2019GL086577>, 2020.

664 Yamazaki, Y., Matthias, V., and Miyoshi, Y.: Quasi-4-day wave: Atmospheric
665 manifestation of the first symmetric Rossby normal mode of zonal wavenumber 2.
666 *Journal of Geophysical Research: Atmospheres*, 126, e2021JD034855.
667 <https://doi.org/10.1029/2021JD034855>, 2021.

668 Yu, F. R., Huang, K. M., Zhang, S. D., Huang, C. M., and Gong, Y.: Observations of
669 eastward propagating quasi 6-day waves from the troposphere to the lower
670 thermosphere during SSWs in early 2016. *Journal of Geophysical Research:*
671 *Atmospheres*, 127, e2021JD036017, <https://doi.org/10.1029/2021JD036017>, 2022.

672

673